

# Optimizing FTQC Programs through QEC Transpiler and Architecture Codesign

Meng Wang  
PNNL and UBC  
Richland, USA  
mengwang@ece.ubc.ca

Chenxu Liu  
PNNL  
Richland, USA  
chenxu.liu@pnnl.gov

Samuel Stein  
PNNL  
Richland, USA  
samuel.stein@pnnl.gov

Yufei Ding  
UCSD  
San Diego, USA  
yufeiding@ucsd.edu

Poulami Das  
UT Austin  
Austin, USA  
poulami.das@utexas.edu

Prashant J. Nair  
UBC  
Vancouver, Canada  
prashantnair@ece.ubc.ca

Ang Li  
PNNL  
Richland, USA  
ang.li@pnnl.gov

## Abstract

Fault-tolerant quantum computing (FTQC) is essential for executing reliable quantum computations of meaningful scale. Widely adopted QEC codes for FTQC, such as the surface code and color codes, utilize Clifford+T gate sets, where T gates are generally considered as the primary bottleneck due to their high resource costs. Recent advances in T gate optimization have significantly reduced this overhead, making Clifford gate complexity an increasingly critical bottleneck that remains largely unaddressed in present FTQC compiler and architecture designs.

To address this new bottleneck, this paper introduces TACO, a Transpiler-Architecture Codesign Optimization framework, to reduce Clifford cost. Specifically, we observe that, through codesign, insights rooted in the FTQC architecture can inform novel circuit-level optimizations for FTQC compilers. These optimizations, in turn, provide new opportunities to redesign and improve the underlying architecture. Evaluations show that TACO achieves an average 91.7% reduction in Clifford gates across diverse quantum circuits and significantly enhances gate parallelism compared to Pauli-based approaches. These improvements enable an efficient FTQC architecture that can achieve single-gate-per-cycle throughput using only  $1.5n + 4$  logical qubit tiles, considerably pushing forward upon previously proposed designs that require  $2n + \sqrt{8n} + 1$  tiles. These results highlight the benefits of bidirectional optimization through codesign. TACO will be open-source.

## 1 Introduction

Quantum computers promise to solve classically intractable problems in many crucial application domains, including large integer factorization [1], database search [2], molecular simulations [3, 4], and more. However, quantum hardware is noisy and the error rates of qubit devices and operations (about 1% of existing systems [5]) far exceed what can be tolerated at the application level (below  $10^{-10}$ ). To bridge this gap, quantum computers employ *Quantum Error Correction (QEC)* codes [6–10] that use redundancy to tolerate errors. QEC codes encode fault-tolerant logical qubits using redundant

Gate Type	Gate Count	Gate Ratio	Baseline Time Cost	Clifford Reduced Time Cost
T	155k	38.7%	311k	311k
S	85k	21.2%	170k	3k (-58×)
H	155k	38.7%	155k	1k (-84.8×)
CX	3k	0.8%	6k	6k
<b>Total</b>	<b>402k</b>	<b>99.4%</b>	<b>644k</b>	<b>322k (-2×)</b>

Table 1: Gates and Time Cost for a 100-Qubit QFT Circuit.

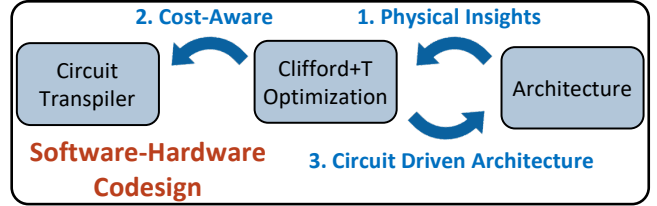
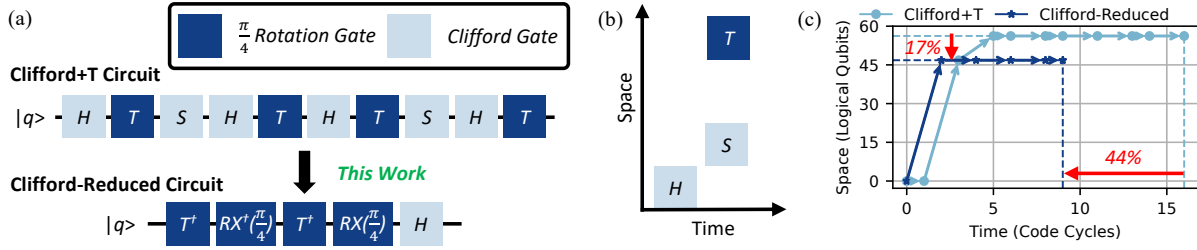


Figure 1: Cross-stack optimization insights: (1) Architecture-guided Clifford+T optimization, (2) Clifford+T-oriented circuit transpilation, and (3) Software-hardware co-design.

physical qubits. A Fault-Tolerant Quantum Computer (FTQC) alternates between operations on logical qubits and QEC cycles. QEC is crucial to unlock the true potential of quantum computing and is being widely studied in both industry and academia, including several demonstrations on real systems in recent years [11–14].

As demonstrated by Eastin-Knill theorem [15], no quantum error correcting code can transversely implement a universal gate set. We consider surface code [10, 16, 17] in this paper as it is one of the most promising QEC codes due to its advantages including its planner local connectivity, high error thresholds, code distance flexibility to adapt logical error requirements, and the availability of polynomial time decoding algorithms for identifying errors.

Surface codes allow fault-tolerant execution of Controlled-Not (CX), Hadamard (H), and Phase (S) gates from the Clifford group, as well as the T gate for non-Clifford operations [16]. The Clifford+T



**Figure 2: Overview of TACO’s Clifford optimization and projected circuit-level Space-Time cost savings from the reduced Clifford operations. (a) Most Clifford gates in the single-qubit Clifford+T circuit can be eliminated. (b) Space-Time cost of Clifford and  $\frac{\pi}{4}$  rotations. (c) Circuit level Space-Time cost of running Clifford+T versus Clifford-Reduced circuit. Each point denotes a gate execution in the circuit. Note that space costs for T and S are incurred at most once due to resource reusing.**

gate set is universal [18] and typically, the T gates are regarded as the most expensive logical operation as it requires resource-intensive magic state distillation [19]. Depending on the gap between the physical and target error rates, a state distillation process can require 850 to 73,400 logical qubits [20]. Consequently, many prior works optimize for a reduced number of T gates [21–26].

Recent advancements in distillation process optimization [20, 27–29] have significantly reduced the cost of the distillation process. Remarkably, in certain scenarios, the cost of distilling a magic state can be lower than performing a logical Clifford gate on full-distance logical qubits [20]. In this case, the cost of Clifford Gates could not be overlooked. In fact, it is becoming quite significant as a new bottleneck for FTQC execution. Table 1 shows the distribution of different gates and their time cost for a 100-qubit Quantum Fourier Transform circuit decomposed using the Clifford+T gate set. Pauli gates are not included as they can be virtually executed and thus cost-free. We see that it contains approximately 40% of T gates and 60% Clifford gates. Furthermore, our studies show that this ratio is very similar across all benchmark programs. Thus, the Clifford gates also contribute significantly to the total circuit execution cost. Minimizing the Clifford gate overhead leads to a 2X reduction in the final time cost as shown in Table 1. Thus, minimizing the overheads of Clifford gates is crucial, which is the main focus of this work.

**Limitations of prior works:** Current solutions reduce the overheads of Clifford gates by transforming the Clifford+T circuit into an equivalent Pauli circuit [30–34], where all the Clifford gates are commuted to the end of the circuit and merged with measurements. Although this approach effectively eliminates all Clifford gates, it incurs additional costs of introducing multi-qubit  $\frac{\pi}{4}$  rotations<sup>1</sup>. These multi-qubit  $\frac{\pi}{4}$  rotations can greatly limit the parallelism (the number of concurrent gates that can be executed). Moreover, the error rates of multi-qubit logical operations increase with the number of logical qubits involved, which often requires us to use codes with higher redundancies (for greater fault-tolerance) in the end. **Our Proposal:** This paper introduces TACO, a transpiler architecture codesign optimization framework that leverages cross-stack optimization insights shown in Figure 1. Current FTQC execution stacks start with an algorithmic circuit, then transpile it into an

intermediate circuit, and finally synthesize this into a Clifford+T circuit. From this circuit, the hardware architecture is designed.

**Insight 1: Hardware-informed Clifford+T Optimization:** The first cross-stack insight that TACO leverages comes from understanding how physical FTQC architectures can support non-standard operations beyond the traditional Clifford+T gate set. For instance, hardware-native gates like  $RX(\frac{\pi}{4})$  can be directly implemented, leading to circuits with significantly fewer Clifford operations, as illustrated in Figure 2(a). To quantify the benefits of this approach, we analyze the space-time overheads associated with each gate type (Figure 2(b)) and calculate the total space-time cost for both conventional and Clifford-reduced circuits (Figure 2(c)). In our cost analysis, each point represents a single gate operation. While T and S gates require space allocation for state distillation, this space overhead need not be duplicated for subsequent instances of these gates in the sequence. Even in this simple example, the Clifford-reduced circuit achieves a 17% reduction in space cost and a 44% decrease in execution time.

**Insight 2: Cost-Aware Circuit Transpilation:** The conversion of algorithmic circuits to Clifford+T format requires two steps: circuit transpilation followed by synthesis. Traditional transpilation methods have been optimized primarily for Noisy-Intermediate-Scale Quantum (NISQ) systems [18, 35–37], where two-qubit gate operations are approximately ten times more error-prone than single-qubit operations [38]. However, this optimization strategy becomes suboptimal in the FTQC regime, where the cost structure is fundamentally different. For instance, a single-qubit RZ rotation may decompose into hundreds of Clifford+T gates, while a two-qubit CX gate, being a native Clifford operation, can be implemented directly. This sharp difference in gate costs necessitates the development of an FTQC-specific transpiler that optimizes for overall Clifford+T complexity rather than simply minimizing two-qubit operations.

**Insight 3: Efficient Hardware-Software Codesign Architecture:** The combination of physical architecture insights and our FTQC-oriented circuit transpiler produces highly structured quantum circuits with predictable patterns of computation and data movement (as illustrated in Figure 8(a)). This structured organization creates an opportunity for optimized hardware design through a feedback loop between software and hardware layers.

<sup>1</sup>Note that the T gate itself is  $\frac{\pi}{4}$  rotation around Z-axis, other  $\frac{\pi}{4}$  rotations include X and Y axis rotations can be applied in the same way as a T gate.

By analyzing the resource utilization patterns in these transpiled circuits, we can identify which qubits require intensive computational resources and which are primarily used for storage. This insight enables an architecture that intelligently allocates physical resources: dedicating expanded regions with robust error correction and high connectivity for computation-intensive qubits, while maintaining a more compact layout for storage-focused qubits. The resulting hardware design is inherently matched to the characteristics of the optimized circuits it will execute.

This closed-loop codesign optimization creates a virtuous cycle: the hardware architecture informs circuit optimization for the compiler, and the optimized circuits reveal unique resource utilization patterns, which can reversely guide specific architectural refinements, as shown in Figure 8. The end result is a tightly integrated hardware-software solution that maximizes the efficiency of both components while minimizing overall resource requirements.

Overall, at the Clifford+T optimization level, TACO achieves a dramatic 91.7% reduction in Clifford gate count. The FTQC-oriented circuit transpiler layer further reduces the total Clifford+T gate count by a factor of 1.37 $\times$ . Furthermore, given that the Clifford-Reduced circuit from TACO exhibits a high locality of  $\frac{\pi}{4}$  rotations on the same qubit, we propose an optimized FTQC architecture specifically designed to efficiently handle these localized rotation sequences. Our architecture achieves a logical gate throughput of 1 gate per QEC code cycle while requiring only  $1.5n + 4$  logical qubit tiles, where  $n$  is the number of logical qubits. This represents a significant improvement over prior work requiring  $2n + \sqrt{8n} + 1$  tiles [31], with the reduction in tile count directly translating to lower physical qubit overheads.

In summary, this work’s **key contributions** are:

- We make the key observation that Clifford gates introduce significant time costs in FTQCs.
- We propose TACO that exploits the unique FTQC circuit structure and achieves over 91.7% reduction in Clifford gate overhead.
- TACO employs a cross-stack gate decomposition algorithm that further reduces total gate overhead by 1.37 $\times$ .
- We demonstrate that a hardware-software codesign leads to a highly space-efficient FTQC architecture - requiring only  $1.5n + 4$  tiles, improving upon prior designs requiring  $2n + \sqrt{8n} + 1$  tiles.

## 2 Background

### 2.1 Quantum Errors and Error Correction Codes

Quantum computing operates with qubits, which exist in a superposition of basis states. For example, a qubit may be mathematically denoted using  $|\psi\rangle = \alpha|0\rangle + \beta|1\rangle$ . However, qubits are imperfect and highly error-prone. A qubit may encounter bit-flip errors (X errors) that change  $|\psi\rangle$  to  $\alpha|1\rangle + \beta|0\rangle$ , or phase-flip errors (Z errors), which alter  $|\psi\rangle$  to  $\alpha|0\rangle - \beta|1\rangle$ , or both (Y errors).

QEC codes encode a logical qubit into multiple physical qubits. The physical qubits correspond to two groups—data qubits that encode the quantum information, and parity qubits that extract information about errors in the form of failed parity checks. The parity information is then used to detect errors and correct them before they accumulate. Stabilizer codes [8], such as surface codes, use parity or *syndrome qubits* to measure *stabilizers*, where are

operators that check the parity of data qubits. X-stabilizers detect Z errors by measuring data qubits in the X basis, whereas Z-stabilizers detect X errors by measuring in the Z basis.

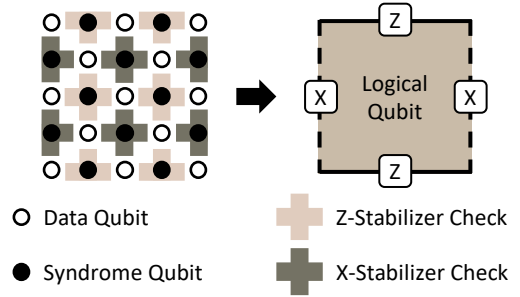


**Figure 3: Distance-3 surface code layout showing data qubits (○), syndrome qubits (●), stabilizers (shaded areas), and logical qubit abstraction. X-stabilizers and Z-stabilizers are represented by different shaded colors.**

The surface code [16, 39, 40] is known for its local topological structure, high error thresholds, and compatibility with universal quantum operations. Figure 3 shows a surface code patch in which qubits are arranged on a 2D lattice, with interleaved data (○) and syndrome qubits (●). The shaded regions denote X and Z stabilizer checks, where each syndrome qubit measures the parity of its adjacent data qubits in either the X or Z basis.

The surface code patch can be abstracted as a logical qubit that is capable of correcting up to  $\frac{d-1}{2}$  errors, where  $d$  is the code distance. For example, the layout in Figure 3 has a distance of 3. Logical qubit patches are drawn with X and Z edges. The types of edges corresponding to stabilizer checks at their boundaries. These edges are crucial for multi-qubit logical operations, detailed in Section 2.4.

### 2.2 Fault-Tolerant Gates in FTQC

Not all quantum gates can be implemented fault-tolerantly using all QEC codes [15]. Most codes, including the surface code, natively support Clifford gates, which include Pauli-X, Pauli-Y, Pauli-Z, Hadamard (H), Phase (S), and Controlled-NOT (CX) gates [16]. However, Clifford gates alone are not sufficient for universal quantum computing [41]. The addition of the non-Clifford *T gate* to the Clifford set achieves universality. Implementing T gates in FTQC, however, is challenging because they are realized using *magic state injection*. Magic state injection involves preparing an ancillary qubit in the *magic state* ( $|M\rangle$ -state).

Magic states are prepared using an extremely resource-intensive process, known as *magic state distillation* [19, 20, 42, 43]. This process demands substantial physical resources. For instance, at a physical qubit error rate of  $p^{-3}$ , preparing a magic state with infidelity below  $10^{-10}$  would require approximately 46,800 logical qubits [20]. Such large resource demands underscore the importance of minimizing the usage of T gates in quantum circuits to enable more resource-efficient FTQCs. Similarly, the Phase gate from the Clifford group also requires state injection from a  $|Y\rangle$ -state. The distillation of  $|Y\rangle$ -state is less expensive in terms of resource overheads as compared to  $|M\rangle$ -state [16, 31].

### 2.3 Circuit Synthesis into the Clifford+T Gates

Quantum programs or circuits must be transpiled into the Clifford+T gate set for execution on an FTQC. We focus on single-qubit unitary decomposition because any multi-qubit operations can be exactly decomposed into CX gates plus single-qubit operations [44]. However, not all single-qubit unitaries can be exactly synthesized using the Clifford+T gate set; most of them require approximation. The Solovay-Kitaev algorithm [45, 46] was first proposed to efficiently approximate arbitrary unitaries, requiring only  $O\left(\log^c\left(\frac{1}{\epsilon}\right)\right)$  gates to achieve an approximation error  $\epsilon$ , where  $c$  is a constant. This algorithm accepts any unitary gates as input and produces sequences in any universal gate set, provided that all gates in the set have their inverses also presented in the set. However, the constant  $c$  has been shown to be around 3.97 [46], implying significant overhead in gate counts.

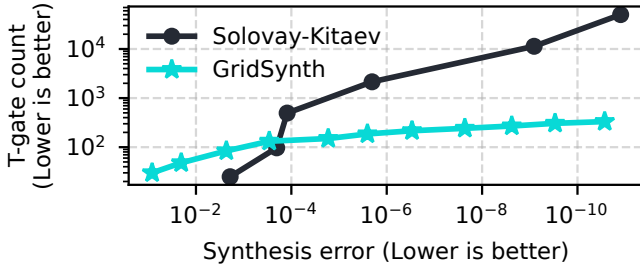


**Figure 4: T-gate count versus synthesis error when synthesizing a random 1-qubit unitary into Clifford+T gate sequence using Solovay-Kitaev algorithm and GridSynth.**

Subsequent works, specifically GridSynth [23], have adopted number-theoretic methods to largely reduce the T-gate count scaling. As shown in Figure 4, to achieve a synthesis error below  $10^{-10}$ , GridSynth requires 332 T gates, whereas the Solovay-Kitaev algorithm requires 50,205 T gates—more than two orders of magnitude higher. Hence, GridSynth is preferred and will be used in our framework. GridSynth restricts the input unitaries to rotation gates along the Z-axis (i.e., RZ gates).

### 2.4 Lattice Surgery in Surface Codes

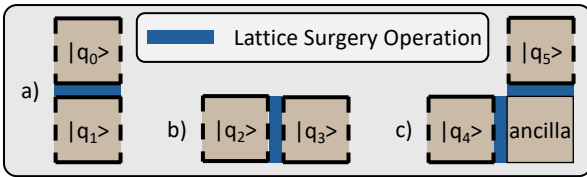


**Figure 5: Lattice surgery operations: (a) ZZ operation for neighboring logical qubits; (b) XX operation for neighboring logical qubits; (c) XZ operation for non-neighboring logical qubits using an ancilla logical qubit.**

Lattice surgery [17, 47, 48] is a prominent technique to perform logical operations in the surface code. It includes merging and splitting logical qubits along their edges by modifying the lattice

configuration and performing targeted measurements. Merging occurs when two logical qubits are joined along a common edge to interact. For instance, merging along X or Z edges facilitates different types of interactions. Splitting reverses this process, separating a merged logical qubit back into individual qubits.

For lattice surgery to work, the edges of the logical qubits involved must be adjacent. If not, the logical qubits must be *moved* or *rotated* to align with the appropriate edges. Alternatively, *ancillary logical qubits* can serve as intermediaries, enabling operations between qubits that are not directly adjacent. Figure 5 illustrates examples of lattice surgery operations for both neighboring and non-neighboring qubits.

## 3 Motivation

### 3.1 Structured Clifford+T Circuit

A foundational theorem in FTQC gate synthesis establishes:

**THEOREM 1.** *Any single-qubit Clifford+T gate sequence can be expressed in Matsumoto-Amano (MA) Normal Form:*

$$\text{MA Normal Form} := (T|\epsilon)(HT|SHT)^*C$$

*This Normal Form exists, is unique, and achieves minimal T-gate count for every single-qubit Clifford+T gate sequence.*

For a complete proof of Theorem 1, please refer to their original paper [49] and its comprehensive review [50]. The significance of the MA Normal Form stems mainly from its guarantee of the optimal T gate count.

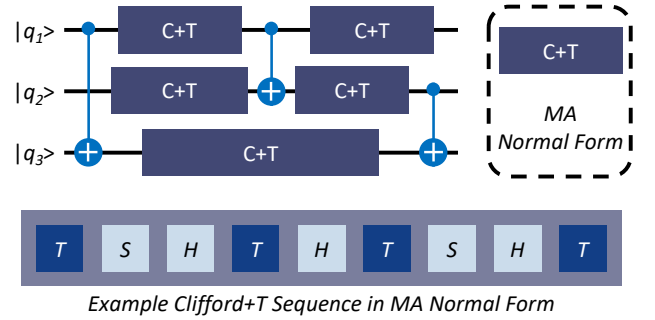


**Figure 6: Standard form of Clifford+T circuits, with all single-qubit operations written in MA Normal Form. Below the circuit is an example of the single-qubit gate sequence.**

In the MA Normal Form, the T, H, S, and C refer to  $\frac{\pi}{4}$ , Hadamard, Phase, and Clifford gates respectively. In this form,  $(T|\epsilon)$  denotes an optional initial T gate, followed by  $(HT|SHT)^*$  which permits any number of consecutive HT or SHT gate combinations. The sequence terminates with a final Clifford gate. Given that FTQC circuits consist exclusively of Clifford+T gates, they can be transformed into the standard form as illustrated in Figure 6, where all single-qubit gate sequences are in the MA Normal Form. As a result, all the FTQC circuits can be represented in a highly structured format that guarantees the optimal T-gate count.

### 3.2 Space-Time Cost of Logical Operations

One key metric for measuring the cost of a logical operation is the *Space-Time cost*. In this metric, space is measured in the number of logical qubits, and time is measured in code cycles, where one code cycle performs one full round of stabilizer checks. While the T gates are deemed as the most expensive gate within Clifford+T gates, their cost is mainly from the costly magic-state on the space vector [20, 42]. In terms of the time cost, the execution time of the T gate, which is the time to inject a distilled magic state to the target qubit state for the T gate, is comparable to a Clifford gate [17].

**Table 2: Space-Time cost of logical operations.**

Gate	Time Cost (cycles)	Space Cost (qubits)
Pauli-(X, Y, Z)	0	0
CX	2	$0.5x-2x$
H	1-4	0
S	2	$9.4x$
T	2	$46.8x$

Specifically, the Pauli gates (X, Y, Z) can be applied virtually [16], making them essentially free. The CX gate can be implemented using lattice surgery, requiring 2 code cycles in total – one each for merging and splitting. While the CX gate typically doesn't require additional ancillary qubits for neighboring qubits, long-distance CX operations may incur architecture-dependent space overhead ranging from  $0.5x$  to  $2x$  [31]. The Hadamard gate can be executed in 1 cycle, but rotating the logical edges of the qubit back to its original layout may require up to 3 additional cycles. Both T and S gates require state injection, which can be performed in 2 cycles, though state preparation involves substantial space costs. For a 1000-qubit algorithm using the state distillation protocol discussed in Section 2.2, the T gate requires approximately  $46.8x$  qubits of space, while the S gate typically requires 20% of the T gate's space cost in Lattice Surgery [31, 51],  $\sim 9.4x$  qubits of space. These costs are summarized in Table 2. Consequently, minimizing the Clifford gates can bring significant improvement for an FTQC execution.

### 3.3 Fundamental Differences in Transpilation: NISQ vs. FTQC

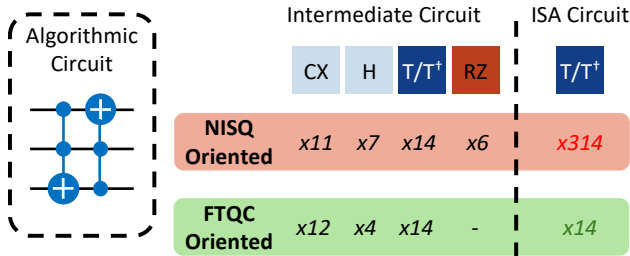


**Figure 7: T gate count in the final Clifford+T circuit when using NISQ or FTQC oriented circuit transpilations.**

Quantum circuit transpilation priorities differ fundamentally between NISQ and FTQC contexts. NISQ devices focus on minimizing

two-qubit gates and treat RZ rotations as nearly free operations. However, in FTQC, each RZ rotation requires approximately 50 T gates, 50 H gates, and 30 S gates for a fault-tolerant implementation. This difference leads to contradictory optimization strategies, as illustrated in Figure 7. While NISQ-oriented optimizations might reduce one CX gate by adding six RZ gates, this seemingly beneficial transformation in the NISQ context actually introduces about 300 additional T gates in the final FTQC circuit. This exemplifies why FTQC-oriented circuit transformations, which consider the full cost of fault-tolerant implementations, are essential yet overlooked by current NISQ-oriented quantum compilers such as Qiskit [37].

## 4 Design of TACO

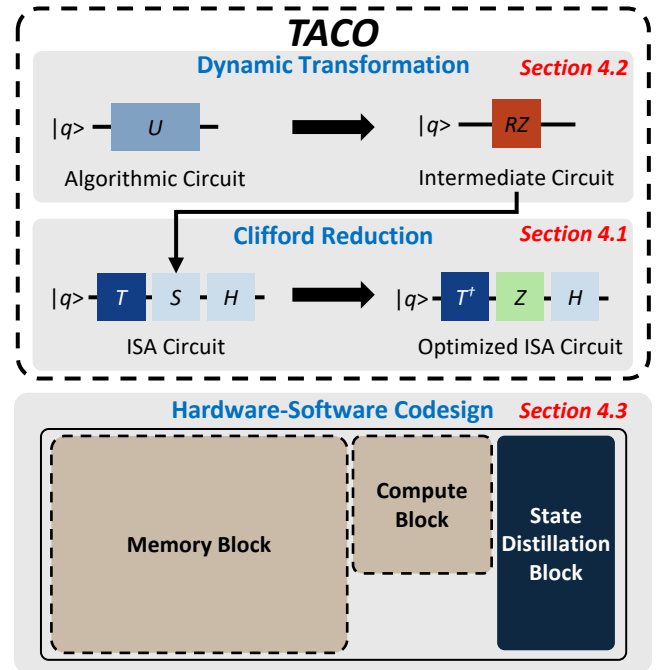


**Figure 8: Overview of TACO framework.** TACO begins with a dynamic gate decomposition of the Algorithmic circuit, transforming it into an intermediate circuit with minimized RZ gates. After synthesizing these RZ gates and generating a Clifford+T circuit, TACO performs a Clifford reduction to reduce the overall time complexity. The resulting optimized circuit demonstrates a high locality of  $\frac{\pi}{4}$  rotations, which motivates a software-guided hardware architecture design.

TACO is a full-stack FTQC optimization framework that addresses optimizations across all three layers of the FTQC execution stack. Figure 8 presents an overview of TACO. We first demonstrate a method to substantially reduce single-qubit Clifford operations in Section 4.1. In Section 4.2, we then introduce a dynamic circuit transformation technique that minimizes high-cost gates during gate synthesis. These optimizations result in an FTQC circuit with enhanced locality, which motivates an efficient FTQC architectural design discussed in Section 4.3.

#### 4.1 Single-Qubit Clifford Operation Reduction

In Clifford+T circuits, T gates typically constitute 40% of total gates, with Clifford gates making up the remaining 60%. While T gates incur the highest cost, this is primarily in terms of space complexity – they demand substantial physical qubit resources for magic state distillation. However, the temporal cost of T gate implementation, once a magic state is well prepared, becomes comparable to that of Clifford gates. This means the 60% proportion of Clifford gates would essentially introduce significant execution time overhead. Since CX gates only account for about 1% of the total Clifford operations, our major optimization efforts concentrate on reducing the remaining single-qubit Clifford operations.

**4.1.1 Eliminating Phase Gates.** Given that the T-count optimality is guaranteed by the MA Normal Form, we focus on reducing the second most costly gate: the **Phase** gate. In MA Normal Form, only two fundamental gate patterns can appear – *HT* and *SHT*, which can yield four possible combined patterns in the sequence:

$$HT HT; HT SHT; SHT HT; SHT SHT \quad (1)$$

A key observation here is that *S gates are consistently preceded by T gates throughout these patterns, with one potential exception: an initial SHT sequence.* We address this special case in Section 4.3.5. A crucial equivalence exists between TS gates and  $T^\dagger Z$  gates, which we can verify through their matrix representations:

$$TS = \begin{bmatrix} 1 & 0 \\ 0 & e^{i\pi/4} \end{bmatrix} \begin{bmatrix} 1 & 0 \\ 0 & i \end{bmatrix} = \begin{bmatrix} 1 & 0 \\ 0 & e^{i\pi/4} \cdot i \end{bmatrix} = \begin{bmatrix} 1 & 0 \\ 0 & e^{i(3\pi/4)} \end{bmatrix} \quad (2)$$

$$T^\dagger Z = \begin{bmatrix} 1 & 0 \\ 0 & e^{-i\pi/4} \end{bmatrix} \begin{bmatrix} 1 & 0 \\ 0 & -1 \end{bmatrix} = \begin{bmatrix} 1 & 0 \\ 0 & -e^{-i\pi/4} \end{bmatrix} = \begin{bmatrix} 1 & 0 \\ 0 & e^{i(3\pi/4)} \end{bmatrix} \quad (3)$$

The identical matrix representations demonstrate that  $TS = T^\dagger Z$ . Note  $T^\dagger$  and Z gates are natively supported on hardware, with Z gates being executed virtually. With this equivalence, we can effectively transform all expensive S gates into 'free' Z gates. The sample gate sequence shown in Figure 6 can be transformed into the new sequence shown in Figure 9.

**4.1.2 Eliminating All Pauli Gates.** Next, once we eliminate all S gates from the sequence, we are left with H, T,  $T^\dagger$ , and Z gates. Although Z gates can be executed virtually, we still want to commute them to the end of the sequence so that the next step of eliminating H gates can be easier. The following commutation relations hold:

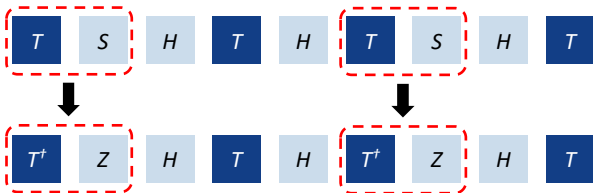


Figure 9: Remove Phase (S) gate using the identity:  $TS = T^\dagger Z$ .

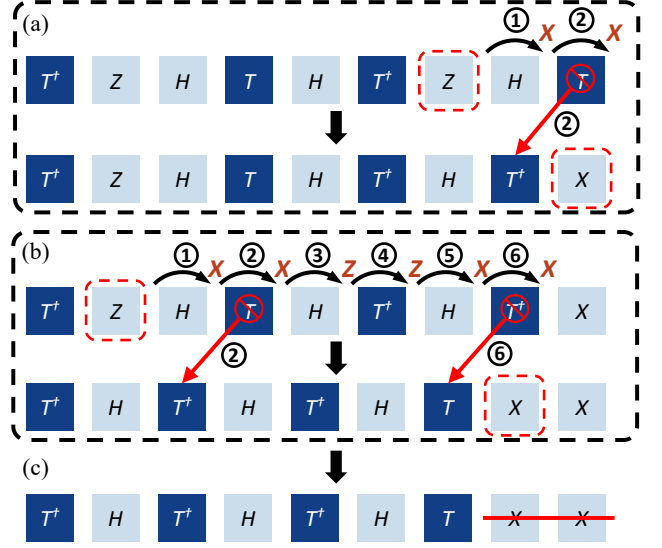


Figure 10: Commute all Pauli-gates to the end of the sequence and merge using commuting rules defined in Equation 4. (a), (b) shows the commuting process of the two Pauli gates and (c) shows the merging of the Pauli gates. Circled numbers indicate the step order.

$$ZH = HX; XH = HZ$$

$$ZT = TZ; ZT^\dagger = T^\dagger Z$$

$$XT = T^\dagger X; XT^\dagger = TX \quad (4)$$

With these commutation relations, all the Pauli gates can be commuted to the end of the sequence and merged together as shown in Figure 10.

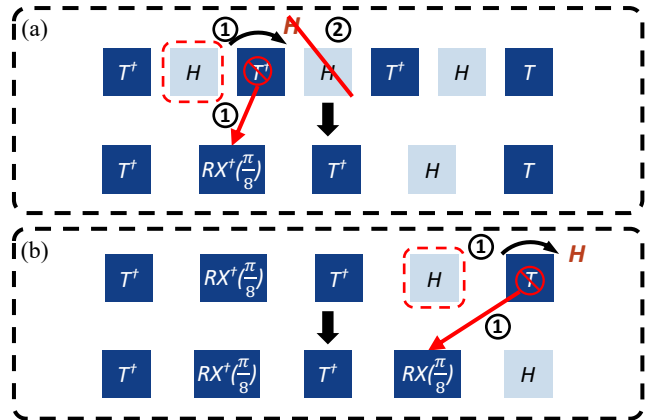


Figure 11: Commuting all the Hadamard gates to the end of the sequence using the commuting rules in Equation 5. Circled numbers indicate the step order.

4.1.3 *Eliminating All Hadamard Gates.* To this point, we also avoid Z. The remaining gates are H, T, and  $T^\dagger$  with a potential Pauli gate at the end of the sequence. Unlike Pauli Gates, Hadamard can not be easily commuted to the end of the sequence. To further eliminate Hadamard gates, we introduce a new gate operator:  $RX(\frac{\pi}{4})^2$ . The following commutation relation holds:

$$\begin{aligned} HT &= RX\left(\frac{\pi}{4}\right)H \\ HT^\dagger &= RX^\dagger\left(\frac{\pi}{4}\right)H \\ HH &= I \end{aligned} \quad (5)$$

To be more efficient, we start with the first Hadamard Gate (the leftmost one) in the sequence and commute it through the sequence. If it meets a T or  $T^\dagger$ , we commute it using the rules above. If it meets another H gate, those two can cancel with each other and we can proceed to the next H gate and repeat this process until reaching the end of the sequence. This process is depicted in Figure 11.

Gate	$RX(\frac{\pi}{4})$ from RZ	$RX(\frac{\pi}{4})$	CX
Count	2,550	8	43
Ratio	98%	0.3%	1.7%

**Table 3: Gate distribution in the 9-qubit Quantum Phase Estimation circuit after optimization.**

4.1.4 *Locality in Optimized Circuit.* After applying the three Clifford+T gate sequence optimizations, we obtain an optimized sequence exhibiting very high ‘locality’—that is, sequences of  $R(\frac{\pi}{4})$  gates are applied to the same qubit. Profiling the 9-qubit Quantum Phase Estimation circuit, shown in Table 3, reveals that over 98% of the  $R(\frac{\pi}{4})$  gates are produced by RZ gate synthesis. As demonstrated in Figure 4, synthesizing a single RZ gate can result in tens or even hundreds of  $R(\frac{\pi}{4})$  gates, depending on the chosen synthesis error threshold. Therefore, most of the  $R(\frac{\pi}{4})$  gates in the circuit exhibit high locality, being sequentially applied to the same qubits. This high degree of locality motivates our new FTQC architecture design to be presented in Section 4.3.

## 4.2 Dynamic Circuit Transformation

Converting quantum gates to Clifford+T gates often requires an intermediate transformation step. The approach used during this transformation significantly impacts the number of RZ gates generated, which subsequently influences the T-gate count in the final circuit. The majority of T gates are from these RZ gates, which in turn have a substantial impact on the final circuit.

Two factors control this transformation: the basis gate set and optimization passes. To evaluate their impact, we analyzed two 4-qubit Quantum Phase Estimation circuits, each estimating the phase of a 2-qubit random unitary. We tested three basis gate sets: Clifford+T+RZ, Clifford+T+U (where U represents generic single-qubit rotations that decompose into RZ gates), and Clifford+T+U+RZ.

<sup>2</sup>Note that T gate itself is equivalent to  $RZ(\frac{\pi}{4})$ , we show later that such RX rotations can be implemented on the hardware equally complex as compared to T gates.

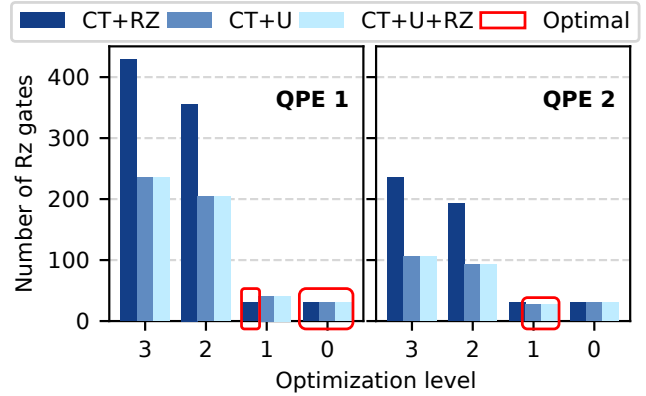


**Figure 12: Number of RZ gates in intermediate circuits obtained from transpiling two 4-qubit QPE circuits using Qiskit Transpiler across optimization levels 0-3 and three basis gate sets (Clifford+T+U, Clifford+T+RZ, Clifford+T+U+RZ). Lower RZ gate counts indicate better optimization.**

Using Qiskit’s circuit transpiler with optimization levels 0-3, we compared the resulting RZ gate counts, shown in Figure 12.

Our results reveal that, *higher optimization levels, which are primarily designed for NISQ devices, can essentially degrade circuit performance for FTQC.* Additionally, no single combination of basis gate set and optimization level consistently produces optimal results across both test circuits.

We present an FTQC-oriented approach to circuit transformation that optimizes quantum circuits based on FTQC-specific considerations. Our method is motivated by two key observations: first, any quantum circuit is ultimately expressed in terms of CX and single-qubit gates for a fault-tolerant implementation. Second, since optimizations across CX gates offer limited benefits for FTQC metrics, we can focus on optimizing sequences of single-qubit gates independently. Based on these insights, our method operates via four key stages:

- (1) First, the algorithm decomposes multi-qubit gates into equivalent sequences of CX and single-qubit gates. This initial decomposition is a necessary step as all quantum operations should ultimately be expressed in this form.
- (2) Second, the algorithm identifies all sequences of single-qubit gates between CX operations. Since optimizations across CX gates are not beneficial for our FTQC metrics, these sequences represent natural boundaries for optimization.
- (3) Third, each identified single-qubit gate sequence undergoes comprehensive optimization independently. This localized approach simplifies the optimization process while capturing the most impactful opportunities for improvement.
- (4) Finally, our method evaluates each optimization using an FTQC-specific metric – *the number of RZ gates*. Optimizations are only accepted if they reduce the RZ gate count, ensuring all transformations directly benefit a fault-tolerant implementation.

We evaluated our proposed method using the same two 4-qubit QPE circuits discussed earlier. As shown in Table 1, our FTQC-oriented dynamic transformation method consistently achieves

Circuit	Qiskit Best Result	TACO
QPE-1	30	30
QPE-2	27	27

**Table 4: RZ gate counts of two QPE circuits.**

optimal RZ gate counts for both test circuits, outperforming the various combinations of basis gates and optimization levels using Qiskit’s transpiler.

### 4.3 High-Locality Architectural Design

The optimized Clifford+T circuit from Section 4.1 exhibits significant locality in  $\frac{\pi}{4}$  rotations applied to individual qubits. The length of these repeated rotation sequences strongly correlates with the chosen synthesis error threshold. These sequences typically extend to dozens or hundreds of consecutive rotations.

Leveraging this high-locality property, we propose an FTQC architecture comprising a memory block and a compute block. The compute block is dedicated to logical qubits requiring long sequences of  $\frac{\pi}{4}$  rotations, with each rotation taking at most one code cycle. The memory block, on the other hand, stores the remaining logical qubits in a compact design. While this design prioritizes space efficiency, it also supports gate execution on these qubits, albeit with a lower throughput.

**4.3.1 Compute Block.** The compute block is primarily designed for qubits undergoing sequences of  $\frac{\pi}{4}$  rotations. In the Clifford-Reduced circuit from Section 4.1, there are four types of  $\frac{\pi}{4}$  rotations: Z-axis rotations, X-axis rotations, and their inverses. The  $RZ(\frac{\pi}{4})$  gate, equivalent to the T gate, requires lattice surgery between a magic state qubit and the Z-edge of the target qubit. Similarly, the  $RX(\frac{\pi}{4})$  gate requires interaction with the X-edge of the target qubit.

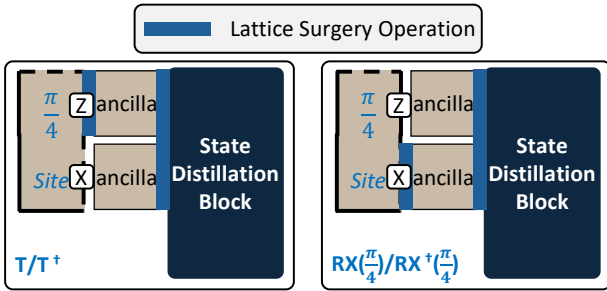


**Figure 13: Layout of the compute block, showing the  $\frac{\pi}{4}$  logical qubit site with both X and Z edges exposed via ancilla qubits to the state distillation block. This configuration supports  $RZ(\frac{\pi}{4})$  (left) and  $RX(\frac{\pi}{4})$  rotations (right) by enabling selective edge interaction. One compute block takes 4 logical qubit tiles - two for the  $\frac{\pi}{4}$  size and 2 ancilla tiles.**

As shown in Figure 13, the compute block includes a dedicated  $\frac{\pi}{4}$  logical qubit site with both its X and Z edges exposed, via ancilla qubits, to the state distillation block. These edges can be selectively activated based on the required operation. During state injection, a regular  $\frac{\pi}{4}$  rotation is applied half of the time, and its inverse

is applied the other half. Such operations can be corrected to the desired rotation using Pauli corrections, which are efficient and cost-free to implement. A compute block takes 4 logical tiles - two for the  $\frac{\pi}{4}$  size plus 2 ancilla tiles

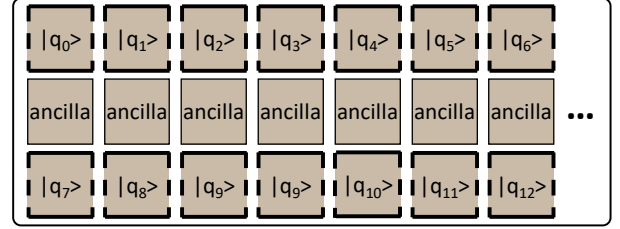


**Figure 14: Memory block layout for storing idle qubits. Logical qubits occupy the first and third rows, while the middle row is reserved for ancilla qubits.**

**4.3.2 Memory Block.** The memory block is designed for storing the remaining qubits. These qubits are mostly idle, except for cases where CX gates or single Hadamard gates need to be applied. We adopt the compact tile design from prior work [31]. Its layout is shown in Figure 14.

In this layout, there are three rows: the first and third rows are occupied by logical qubit tiles, while the middle row is reserved for ancilla qubits. The total space cost of the memory block is  $1.5n$ , where  $n$  is the number of logical qubits. This design allows any pair of qubits to directly access each other via the ancilla qubits, making CX gates between any pair of logical qubits feasible. Additionally, Hadamard gates can be applied locally without additional overhead.

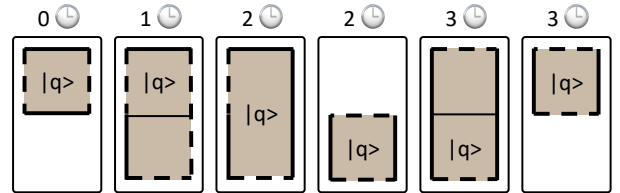


**Figure 15: Patch rotation process in the memory block. The process involves expanding and contracting a logical qubit to expose a different edge, taking 3 code cycles in total.**

**4.3.3 Patch Rotation.** In the memory block, each logical qubit has only one edge, either X or Z, exposed to interact with other qubits. Sometimes, a different edge is needed for a specific operation. In such cases, a patch rotation is performed, as shown in Figure 15. During this process, expanding the logical qubit to include neighboring tiles (steps 2, 3, and 5 in the figure) requires 1 code cycle. Conversely, shrinking the logical qubit’s footprint (steps 4 and 6 in the figure) requires no additional time, as it simply involves disabling stabilizer measurements on the unused tiles. Altogether, the patch rotation takes 3 code cycles. These operations are quite occasional, as compared to the frequent  $\frac{\pi}{4}$  rotations occurring in the compute block. As a result, patch rotations in the memory block can be completed without slowing down the compute block.



**4.3.4 Qubit Transfer Between Memory and Compute Blocks.** When a logical qubit needs to be transferred between the memory and compute blocks, the direct access between all storage sites in the memory block and the compute block allows the transfer to be completed in a single code cycle. This involves expanding the qubit to the compute block and then shrinking it back to its operational configuration.

**4.3.5 The Phase Gate.** We have now described all the gate execution procedures except for the phase gate, which might remain after optimizing the single-qubit Clifford+T gate sequence. The phase gate can be executed efficiently using one of two methods:

**Sharing the State Distillation Block** The distillation process for the  $|Y\rangle$  state, required by the phase gate, consumes about 20% of the physical qubit resources needed for the distillation of the  $|M\rangle$  state used in the T gate. The phase gate can only appear at the end of a single-qubit Clifford+T sequence that involves repeated  $\frac{\pi}{4}$  rotations. During this time, the qubits are brought to the compute block for these rotations, allowing the state distillation block to be partially reused to generate the necessary  $|Y\rangle$  state for the single phase gate.

**Decomposing into Two T Gates** If the state distillation block is strictly optimized for  $|M\rangle$  state distillation and cannot support  $|Y\rangle$  state generation, the phase gate can be decomposed into two T gates. Since each sequence can include at most one phase gate, this approach introduces less than a 1% extra overhead in T-gate usage.

## 5 TACO Evaluation Settings

### 5.1 Figure of Merit

To evaluate TACO, we employ a set of well-defined metrics. During the transpilation of circuits into the intermediate Clifford+T+RZ form, we focus on the number of RZ gates in the resulting intermediate circuit. For each benchmark, we normalize the RZ gate count from different transpilation methods relative to the highest count, enabling a fair comparison across methods.

For Clifford Reduction, we assess the percentage reduction in the number of Hadamard and Phase gates. Other Clifford gates are either left unchanged during optimization, such as CX gates, or are considered free of cost, such as the Pauli gates. Additionally, we evaluate potential time savings resulting from this Clifford Reduction using the logical gate times listed in Table 5. For gates with variable time costs, such as the Hadamard gate, we use the average values for the calculations.

Gate	$R(\frac{\pi}{4})$	S	CX	H
Time Cost	2	2	2	2.5

Table 5: Logical Gate Execution Time.

### 5.2 Benchmark Circuits

We include a diverse of FTQC benchmarks from QASMBench [52], as listed in Table 6. The Quantum Fourier Transform (QFT) is the foundational subroutine for many FTQC algorithms, including Shor’s algorithm for integer factorization [1]. The Quantum Phase Estimation (QPE) circuit is crucial for extracting eigenvalues of

Circuit	Number of Qubits	Number of Gates
QFT	18	783
QF21	15	79
ISING	26	307
DNN	33	176
QUGAN	111	438
KNN	341	513
QPE	9	36
W_STATE	76	378

Table 6: Benchmark Circuit Characteristics.

unitary operators, enabling key applications in quantum chemistry, linear equations solving, and quantum simulation.

To ensure comprehensive coverage of different circuit structures and applications, we include several additional benchmarks. The QF21 circuit represents basic quantum functionality testing. The ISING model simulation circuit is essential for studying quantum many-body physics and quantum magnetism. The Deep Neural Network (DNN) implementation demonstrates the potential of quantum-enhanced machine learning algorithms. The QUGAN benchmark explores quantum adversarial learning and data generation capabilities from [53]. The K-Nearest Neighbors (KNN) algorithm implementation represents quantum versions of classical clustering algorithms. Finally, the W-State preparation circuit is included as it represents an important class of entangled quantum states with applications in quantum communication and metrology.

The qubit and gate numbers of the benchmarks are summarized in Table 6. This diverse set of benchmarks spans both fundamental quantum algorithms and practical applications across physics, machine learning, and quantum information processing, providing a comprehensive test suite for evaluating quantum computing systems across different computational paradigms.

### 5.3 Clifford+T+RZ Transpilation

We compare our dynamic circuit decomposition method, TACO, with Qiskit across three basis gate sets: *Clifford+T+RZ*, *Clifford+T+U*, and *Clifford+T+U+RZ*. For all comparisons, we use Qiskit’s optimization level 1, as it has been shown to provide the best performance.

Beyond individual comparisons with each of the three basis gate sets, we also introduce an *ensemble mode*. In this mode, for each benchmark, we select the best result among the three basis gate sets, effectively combining their strengths. This additional comparison allows us to evaluate how TACO performs not only against specific transpilation strategies but also against an optimized baseline that leverages the best possible outcome from a NISQ transpiler.

The Clifford gates include CX, H, S,  $S^\dagger$ , and the Pauli gates X, Y, and Z. The T gates consist of T and its inverse  $T^\dagger$ . The U gate represents a generic single-qubit rotation gate, which can be decomposed into at most three RZ gates and two H gates. Finally, the RZ gate performs a rotation around the Z axis and can be further synthesized into the *Clifford+T* basis in subsequent steps.

### 5.4 Clifford+T Synthesis

The *Clifford+T* circuits for the benchmarks are generated using the GridSynth algorithm [23]. Specifically, GridSynth is employed to

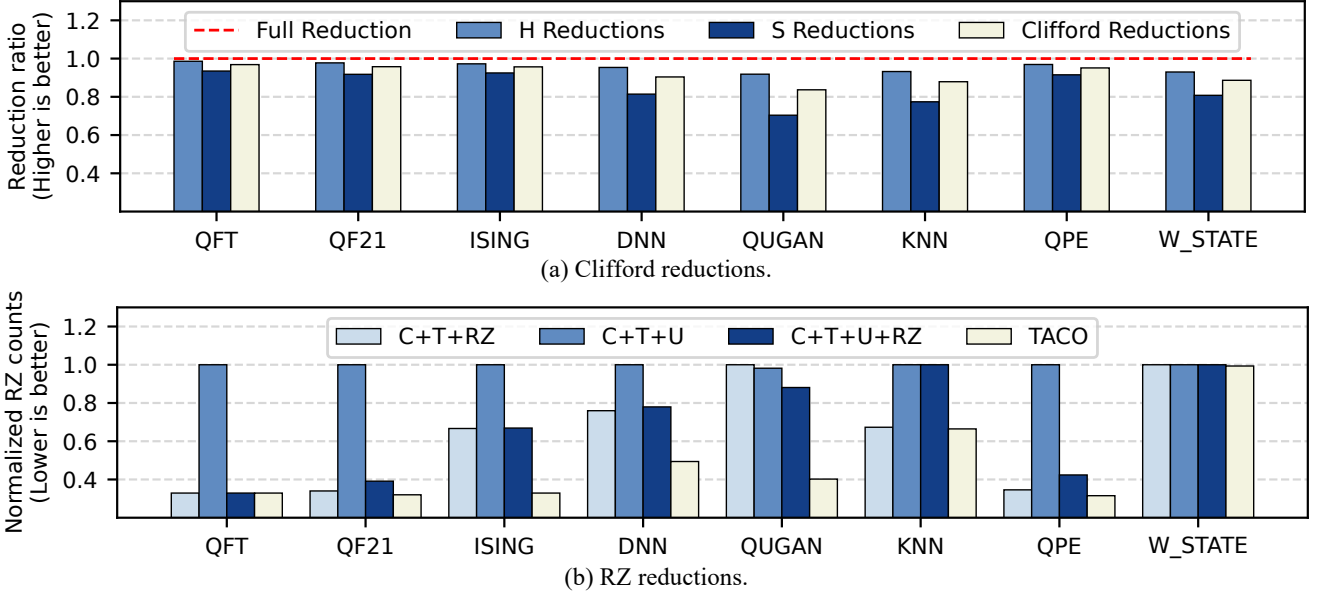


**Figure 16: Performance evaluation of TACO: (a) Reduction ratios for H gates, S gates, and total Clifford gates across benchmark circuits. A higher ratio indicates a greater reduction. (b) Comparison of normalized RZ gate counts achieved by TACO versus three NISQ transpilation approaches using different basis gate sets. Lower counts indicate better performance.**

synthesize RZ gates into sequences of *Clifford+T* gates. For this process, a synthesis error tolerance of  $10^{-5}$  is used, ensuring high-precision approximations while maintaining a balance between circuit depth and accuracy.

## 6 TACO Evaluation Results

We evaluate TACO across three key dimensions: (1) Clifford gate reduction capability compared to standard Clifford+T circuits, (2) total RZ gate reduction prior to Clifford+T synthesis, and (3) resulting performance improvements from Clifford reduction.

### 6.1 Clifford Reduction

Figure 16(a) shows our reduction results for H gates, S gates, and total Clifford gates across all benchmark circuits. TACO achieves average reductions of 95.5% for H gates, 84.9% for S gates, and 91.7% for total Clifford gates.

The results are particularly striking for key FTQC subroutines: QFT circuits show 98.6% H-gate and 93.5% S-gate reductions, while QPE circuits demonstrate 96.9% H-gate and 91.5% S-gate reductions. These translate to over 31x and 20x total Clifford gate reductions for QFT and QPE respectively compared to Clifford+T baselines.

The exceptional performance can be attributed to TACO’s ability to identify and optimize common quantum arithmetic patterns. In QFT circuits, the standard implementation requires numerous Hadamard gates for basis transformations and controlled-phase rotations. Our approach recognizes these patterns and consolidates multiple rotation operations, significantly reducing the Hadamard gate count. Similarly, for QPE circuits, the reduction in S gates stems

from our optimization of phase estimation sequences, where consecutive phase rotations are merged into more efficient composite operations.

### 6.2 RZ Reduction

Since RZ synthesis accounts for over 99% of Clifford+T gates in typical circuits, reducing RZ gate count provides substantial benefits. Figure 16(b) compares TACO’s dynamic circuit transpilation method against three NISQ transpilation approaches. TACO consistently achieves optimal results, reducing RZ counts by factors of 1.4x, 2.4x, and 1.5x compared to NISQ transpilation using *Clifford+T+RZ*, *Clifford+T+U*, and *Clifford+T+U+RZ* basis sets respectively. Even when compared to an ensemble approach that selects the best result from multiple NISQ transpilation runs with different basis sets, TACO maintains a 1.37x reduction advantage.

The *W\_state* circuit presents an interesting case where all transpilation methods achieve identical results. Upon analysis, this circuit contains only RY gates (decomposable to a single non-trivial RZ gate and two H gates), CZ gates (decomposable to two CX plus one RZ), and Clifford gates (CX and X), allowing all methods to trivially discover the optimal decomposition.

### 6.3 Time Savings in FTQC Execution

To evaluate the practical impact of our optimizations, we analyzed the total execution time in terms of FTQC cycles for each benchmark circuit. Figure 17 shows the comparison between baseline execution times and those achieved by TACO. Our approach consistently delivers significant improvements across all benchmark circuits, achieving speedups between 2.3x and 2.6x.

The most substantial improvements are observed in QFT and ISING circuits, both achieving 2.6x speedup. This is particularly noteworthy for QFT, as it is a fundamental building block in many quantum algorithms. The QUGAN and KNN circuits show 2.3x improvement, while QPE and W\_STATE demonstrate 2.5x and 2.4x reductions respectively. The DNN circuit achieves a 2.4x speedup, indicating that our optimization technique scales well to more complex neural network implementations.

These time reductions stem directly from our Clifford and RZ gate optimizations, as each eliminated gate reduces the number of physical operations required in the fault-tolerant implementation. The consistency of improvement across diverse circuit types suggests that our optimization strategy is robust and generally applicable to different quantum computing applications.

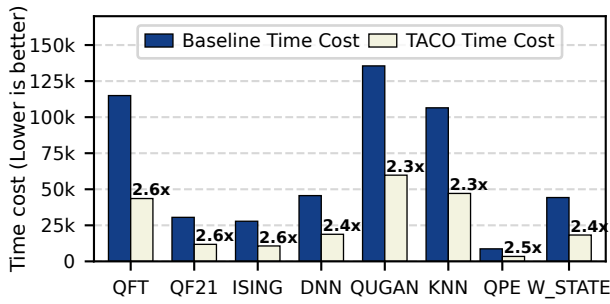


**Figure 17: Comparison of FTQC execution time costs between baseline implementation and TACO across different benchmark circuits. Numbers above the white bars indicate the reduction factor achieved by TACO.**

## 6.4 Improved Parallelism over PBC

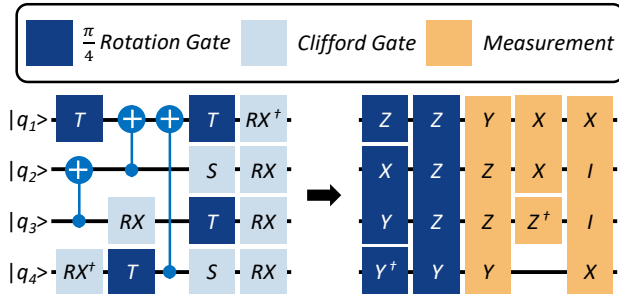


**Figure 18: Example of transforming a Clifford+T circuit (left) into a PBC circuit (right). The RX gates represent  $RX(\frac{\pi}{2})$  rotations, which are Clifford gates. In the PBC circuit, letters indicate qubit edges for lattice surgery, with Y requiring access to both X and Z edges simultaneously.**

PBC [30–34] is an approach designed to fully eliminate the execution overhead of Clifford gates. In PBC, all Clifford gates are commuted to the end of the circuit and merged with the measurement operations. This transformation results in converting a large number of T gates into multi-qubit  $\frac{\pi}{4}$  rotations, as illustrated

in Figure 18. However, these multi-qubit operations significantly constrain the parallelism of  $\frac{\pi}{4}$  rotations, which can substantially degrade some state-of-the-art estimates of FTQC execution times [54].

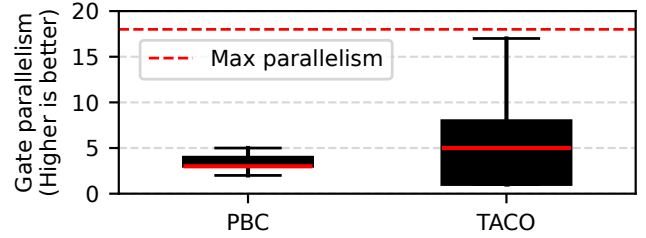


**Figure 19: Gate parallelism of 18-qubit QFT in PBC and TACO.**

To evaluate this effect, we analyzed an 18-qubit QFT circuit. Figure 19 presents a boxplot of gate parallelism—i.e., the number of gates that can be executed concurrently at a given time step. Under PBC, the median parallelism is only 3, with a maximum parallelism of 5. In contrast, using TACO, the median parallelism increases to 5, and the maximum reaches 17—nearly the theoretical maximum for this 18-qubit circuit. Such parallelism is crucial for achieving the practical FTQC execution envisioned for the future [54].

## 7 Related Works

### 7.1 Pauli Based Computation

Pauli-based computation (PBC) is a model for universal quantum computation that removes all the Clifford gate operations in a quantum circuit model and solely utilizes adaptive Pauli measurements and magic state preparation and injection for computation. Ref. [30] proposed the foundational framework of PBC, demonstrating its equivalence to universal quantum computation. Since then, significant progress has been made in exploring this computational model. Litinski applies PBC with fault-tolerant quantum computation and designed surface-code quantum computer architecture [31]. Practical implementations and optimizations of PBC, including techniques for quantum circuit compilation and hybrid computation with reduced resource overheads have been discussed in Ref. [32]. Circuit optimization frameworks inspired by PBC have also been introduced [33]. Furthermore, adapting PBC into higher-dimensional quantum systems is also investigated in Ref. [34].

### 7.2 QEC Codes and Optimization

In this manuscript, we mainly focus on patch-based surface code with lattice surgery for logical operations. There are other types of surface code constructions, including defect-based [16], and twist-based [55] surface code. Specifically, defect-based surface code uses braiding operations to perform logical CX operations, however, with more physical qubit overhead [17, 31].

Other than surface codes, there are several other types of quantum error correction code constructions. Quantum stabilizer codes, such as Shor’s code [6, 56] and Steane’s [57] code, form a class of QEC codes that use a group of stabilizers, to define a protected subspace for logical quantum states. Color codes [58], a type of topological QEC, are widely studied and experimentally demonstrated [13, 59–61], particularly due to their ability to support

transversal Clifford operations. Recently, there has been growing interest in quantum Low-Density Parity-Check (LDPC) codes [62–64], which feature long-range stabilizer checks and offer high code rates, making them attractive for scalable quantum computing.

As demonstrated by Eastin-Knill theorem [15], no quantum error correcting code can transversely implement a universal gate set. In surface code, the T-gate cannot be transversely implemented, hence requiring magic state preparation. In order to prepare a magic state with required error rates, multiple magic state distillation protocols have been proposed, e.g., using Reed-Muller code [19, 65], block codes [42, 43, 66] for error detection to purify the generated magic states. Recently, more works about reducing the magic state purification by optimizing the purification protocol [20, 54, 67] or cultivating the magic state have been proposed [68].

Quantum error correction requires identifying the possible location of errors by syndrome measurements. Locating the error based on the syndrome measurements is the QEC decoding process. The QEC decoding can be achieved by lookup table [69, 70], Minimum Weight Perfect Matching (MWPM) [40, 71], and machine learning methods [72–74]. Among them, MWPM is one of the most efficient decoding algorithms for QEC codes [75–78]. Limited by the space, for a review of recent decoders for surface code, we suggest referring to Ref. [79].

## 8 Conclusion

Fault-tolerant quantum computing (FTQC) implementations use Clifford+T gates, with both contributing significant execution overhead. While T gate implementations have seen recent improvements, Clifford gate optimization remains challenging and crucial. We introduce TACO, a Transpiler-Architecture Codesign Optimization framework that achieves an average 91.7% reduction in Clifford gates across diverse quantum circuits, leading to execution time improvements of up to 2.6x. Compared to Pauli-based computation approaches, TACO more than doubles the gate parallelism and achieves maximum parallelization in specific FTQC execution phases. These advancements are crucial for enabling efficient large-scale FTQC implementations.

## Acknowledgments

This material is based upon work supported by the U.S. Department of Energy, Office of Science, National Quantum Information Science Research Centers, Co-design Center for Quantum Advantage (C2QA) under contract number DE-SC0012704, (Basic Energy Sciences, PNNL FWP 76274). This research was also supported in part by the National Research Council (NRC) Canada grants AQC 003 and AQC 213, as well as the Natural Sciences and Engineering Research Council of Canada (NSERC) [funding number RGPIN-2019-05059]. This research used resources of the Oak Ridge Leadership Computing Facility, which is a DOE Office of Science User Facility supported under Contract DE-AC05-00OR22725. This research used resources of the National Energy Research Scientific Computing Center (NERSC), a U.S. Department of Energy Office of Science User Facility located at Lawrence Berkeley National Laboratory, operated under Contract No. DE-AC02-05CH11231.

## References

- [1] Peter W Shor. Polynomial-time algorithms for prime factorization and discrete logarithms on a quantum computer. *SIAM review*, 41(2):303–332, 1999.

- [2] Lov K Grover. A fast quantum mechanical algorithm for database search. In *Proceedings of the twenty-eighth annual ACM symposium on Theory of computing*, pages 212–219, 1996.
- [3] Richard P Feynman. Simulating physics with computers. In *Feynman and computation*, pages 133–153. cRc Press, 2018.
- [4] Seth Lloyd. Universal quantum simulators. *Science*, 273(5278):1073–1078, 1996.
- [5] Google Quantum AI. Quantum computer datasheet, 2021. <https://quantumai.google/hardware/datasheet/weber.pdf>.
- [6] Peter W Shor. Scheme for reducing decoherence in quantum computer memory. *Physical review A*, 52(4):R2493, 1995.
- [7] A Robert Calderbank and Peter W Shor. Good quantum error-correcting codes exist. *Physical Review A*, 54(2):1098, 1996.
- [8] Daniel Gottesman. *Stabilizer codes and quantum error correction*. California Institute of Technology, 1997.
- [9] Emanuel Knill, Raymond Laflamme, and Gerald J Milburn. A scheme for efficient quantum computation with linear optics. *nature*, 409(6816):46–52, 2001.
- [10] A Yu Kitaev. Fault-tolerant quantum computation by anyons. *Annals of physics*, 303(1):2–30, 2003.
- [11] Jay M Gambetta, Jerry M Chow, and Matthias Steffen. Building logical qubits in a superconducting quantum computing system. *npj quantum information*, 3(1):2, 2017.
- [12] Suppressing quantum errors by scaling a surface code logical qubit. *Nature*, 614(7949):676–681, 2023.
- [13] Dolev Bluvstein, Simon J Evered, Alexandra A Geim, Sophie H Li, Hengyun Zhou, Tom Manovitz, Sepehr Ebadi, Madelyn Cain, Marcin Kalinowski, Dominik Hangleiter, et al. Logical quantum processor based on reconfigurable atom arrays. *Nature*, 626(7997):58–65, 2024.
- [14] Ben W Reichardt, Adam Paetznick, David Aasen, Ivan Basov, Juan M. Bello-Rivas, Parsa Bonderson, Rui Chao, Wim van Dam, Matthew B. Hastings, Andres Paz, Marcus P. da Silva, Aarthi Sundaram, Krysta M. Svore, Alexander Vaschillo, Zhenghan Wang, Matt Zanner, William B. Cairncross, Cheng-An Chen, Daniel Crow, Hyosub Kim, Jonathan M. Kindem, Jonathan King, Michael McDonald, Matthew A. Norcia, Albert Ryou, Mark Stone, Laura Wadleigh, Katrina Barnes, Peter Battaglini, Thomas C. Bohdanowicz, Graham Booth, Andrew Brown, Mark O. Brown, Kayleigh Cassella, Robin Coxe, Jeffrey M. Epstein, Max Feldkamp, Christopher Griger, Eli Halperin, Andre Heinz, Frederic Hummel, Matthew Jaffe, Antonia M. W. Jones, Eliot Kapit, Krish Kotru, Joseph Lauigan, Ming Li, Jan Marjanovic, Eli Megidish, Matthew Meredith, Ryan Morshead, Juan A. Muniz, Sandeep Narayanaswami, Ciro Nishiguchi, Timothy Paule, Kelly A. Pawlak, Kristen L. Pudenz, David Rodríguez Pérez, Jon Simon, Aaron Smull, Daniel Stack, Miroslav Urbaneck, René J. M. van de Veerdonk, Zachary Vendeiro, Robert T. Weverka, Thomas Wilkason, Tsung-Yao Wu, Xin Xie, Evan Zalyz-Geller, Xiaogang Zhang, and Benjamin J. Bloom. Logical computation demonstrated with a neutral atom quantum processor, 2024.
- [15] Bryan Eastin and Emanuel Knill. Restrictions on transversal encoded quantum gate sets. *Phys. Rev. Lett.*, 102:110502, Mar 2009.
- [16] Austin G Fowler, Matteo Mariantoni, John M Martinis, and Andrew N Cleland. Surface codes: Towards practical large-scale quantum computation. *Physical Review A—Atomic, Molecular, and Optical Physics*, 86(3):032324, 2012.
- [17] Dominic Horsman, Austin G Fowler, Simon Devitt, and Rodney Van Meter. Surface code quantum computing by lattice surgery. *New Journal of Physics*, 14(12):123011, 2012.
- [18] Michael A Nielsen and Isaac L Chuang. *Quantum computation and quantum information*. Cambridge university press, 2010.
- [19] Sergey Bravyi and Alexei Kitaev. Universal quantum computation with ideal clifford gates and noisy ancillas. *Physical Review A—Atomic, Molecular, and Optical Physics*, 71(2):022316, 2005.
- [20] Daniel Litinski. Magic state distillation: Not as costly as you think. *Quantum*, 3:205, 2019.
- [21] Vadym Kliuchnikov, Dmitri Maslov, and Michele Mosca. Asymptotically optimal approximation of single qubit unitaries by clifford and t circuits using a constant number of ancillary qubits. *Physical review letters*, 110(19):190502, 2013.
- [22] Vadym Kliuchnikov. Synthesis of unitaries with clifford+ t circuits. *arXiv preprint arXiv:1306.3200*, 2013.
- [23] Neil J Ross and Peter Selinger. Optimal ancilla-free clifford+ t approximation of z-rotations. *arXiv preprint arXiv:1403.2975*, 2014.
- [24] Alex Bocharov, Martin Roetteler, and Krysta M Svore. Efficient synthesis of universal repeat-until-success quantum circuits. *Physical review letters*, 114(8):080502, 2015.
- [25] Matthew Amy and Michele Mosca. T-count optimization and reed-muller codes. *IEEE Transactions on Information Theory*, 65(8):4771–4784, 2019.
- [26] Aleks Kissinger and John van de Wetering. Reducing the number of non-clifford gates in quantum circuits. *Physical Review A*, 102(2):022406, 2020.
- [27] Earl T. Campbell and Mark Howard. Unified framework for magic state distillation and multiqubit gate synthesis with reduced resource cost. *Physical Review A*, 95(2), February 2017.

- [28] Jeongwan Haah, Matthew B Hastings, David Poulin, and D Wecker. Magic state distillation with low space overhead and optimal asymptotic input count. *Quantum*, 1:31, 2017.
- [29] Craig Gidney and Austin G Fowler. Efficient magic state factories with a catalyzed  $|ccz\rangle$  to  $2|t\rangle$  transformation. *Quantum*, 3:135, 2019.
- [30] Sergey Bravyi, Graeme Smith, and John A. Smolin. Trading classical and quantum computational resources. *Phys. Rev. X*, 6:021043, Jun 2016.
- [31] Daniel Litinski. A game of surface codes: Large-scale quantum computing with lattice surgery. *Quantum*, 3:128, 2019.
- [32] Filipa C. R. Peres and Ernesto F. Galvão. Quantum circuit compilation and hybrid computation using Pauli-based computation. *Quantum*, 7:1126, oct 2023.
- [33] Jennifer Paykin, Albert T. Schmitz, Mohannad Ibrahim, Xin-Chuan Wu, and A. Y. Matsuura. Pcoast: A pauli-based quantum circuit optimization framework. In *2023 IEEE International Conference on Quantum Computing and Engineering (QCE)*, volume 01, pages 715–726, 2023.
- [34] Filipa C. R. Peres. Pauli-based model of quantum computation with higher-dimensional systems. *Phys. Rev. A*, 108:032606, Sep 2023.
- [35] Juha J Vartiainen, Mikko Möttönen, and Martti M Salomaa. Efficient decomposition of quantum gates. *Physical review letters*, 92(17):177902, 2004.
- [36] Ville Bergholm, Josh Izaac, Maria Schuld, Christian Gogolin, Shah Nawaz Ahmed, Vishnu Ajith, M Sohaib Alam, Guillermo Alonso-Linaje, B Akash Narayanan, Ali Asadi, et al. PennyLane: Automatic differentiation of hybrid quantum-classical computations. *arXiv preprint arXiv:1811.04968*, 2018.
- [37] Ali Javadi-Abhari, Matthew Treinish, Kevin Krsulich, Christopher J. Wood, Jake Lishman, Julien Gacon, Simon Martiel, Paul D. Nation, Lev S. Bishop, Andrew W. Cross, Blake R. Johnson, and Jay M. Gambetta. Quantum computing with Qiskit, 2024.
- [38] IBM Quantum. About calibration jobs. <https://docs.quantum-computing.ibm.com/admin/calibration-jobs>.
- [39] Sergey B Bravyi and A Yu Kitaev. Quantum codes on a lattice with boundary. *arXiv preprint quant-ph/9811052*, 1998.
- [40] Eric Dennis, Alexei Kitaev, Andrew Landahl, and John Preskill. Topological quantum memory. *Journal of Mathematical Physics*, 43(9):4452–4505, 2002.
- [41] Scott Aaronson and Daniel Gottesman. Improved simulation of stabilizer circuits. *Physical Review A—Atomic, Molecular, and Optical Physics*, 70(5):052328, 2004.
- [42] Sergey Bravyi and Jeongwan Haah. Magic-state distillation with low overhead. *Physical Review A—Atomic, Molecular, and Optical Physics*, 86(5):052329, 2012.
- [43] Cody Jones. Multilevel distillation of magic states for quantum computing. *Physical Review A—Atomic, Molecular, and Optical Physics*, 87(4):042305, 2013.
- [44] Adriano Barenco, Charles H Bennett, Richard Cleve, David P DiVincenzo, Norman Margolus, Peter Shor, Tycho Sleator, John A Smolin, and Harald Weinfurter. Elementary gates for quantum computation. *Physical review A*, 52(5):3457, 1995.
- [45] A Yu Kitaev. Quantum computations: algorithms and error correction. *Russian Mathematical Surveys*, 52(6):1191, 1997.
- [46] Christopher M Dawson and Michael A Nielsen. The solovay-kitaev algorithm. *arXiv preprint quant-ph/0505030*, 2005.
- [47] Austin G Fowler and Craig Gidney. Low overhead quantum computation using lattice surgery. *arXiv preprint arXiv:1808.06709*, 2018.
- [48] Alexander Erhard, Hendrik Poulsen Nautrup, Michael Meth, Lukas Postler, Roman Stricker, Martin Stadler, Vlad Negnevitsky, Martin Ringbauer, Philipp Schindler, Hans J Briegel, et al. Entangling logical qubits with lattice surgery. *Nature*, 589(7841):220–224, 2021.
- [49] Ken Matsumoto and Kazuyuki Amano. Representation of quantum circuits with clifford and pi/8 gates. *arXiv preprint arXiv:0806.3834*, 2008.
- [50] Brett Giles and Peter Selinger. Remarks on matsumoto and amano’s normal form for single-qubit clifford+ t operators. *arXiv preprint arXiv:1312.6584*, 2013.
- [51] Daniel Herr, Franco Nori, and Simon J Devitt. Lattice surgery translation for quantum computation. *New Journal of physics*, 19(1):013034, 2017.
- [52] Ang Li, Samuel Stein, Sriram Krishnamoorthy, and James Ang. Qasmbench: A low-level qasm benchmark suite for nisq evaluation and simulation, 2022.
- [53] Samuel A. Stein, Betis Baheri, Daniel Chen, Ying Mao, Qiang Guan, Ang Li, Bo Fang, and Shuai Xu. Qugan: A quantum state fidelity based generative adversarial network. In *2021 IEEE International Conference on Quantum Computing and Engineering (QCE)*, page 71–81. IEEE, October 2021.
- [54] Craig Gidney and Martin Ekerå. How to factor 2048 bit rsa integers in 8 hours using 20 million noisy qubits. *Quantum*, 5:433, 2021.
- [55] H. Bombin. Topological order with a twist: Ising anyons from an abelian model. *Phys. Rev. Lett.*, 105:030403, Jul 2010.
- [56] Dave Bacon. Operator quantum error-correcting subsystems for self-correcting quantum memories. *Phys. Rev. A*, 73:012340, Jan 2006.
- [57] Andrew Steane. Multiple-particle interference and quantum error correction. *Proceedings of the Royal Society of London. Series A: Mathematical, Physical and Engineering Sciences*, 452(1954):2551–2577, 1996.
- [58] H. Bombin and M. A. Martin-Delgado. Topological quantum distillation. *Phys. Rev. Lett.*, 97:180501, Oct 2006.
- [59] D. Nigg, M. Müller, E. A. Martinez, P. Schindler, M. Hennrich, T. Monz, M. A. Martin-Delgado, and R. Blatt. Quantum computations on a topologically encoded qubit. *Science*, 345(6194):302–305, 2014.
- [60] C. Ryan-Anderson, J. G. Bohnet, K. Lee, D. Gresh, A. Hankin, J. P. Gaebler, D. Francois, A. Chernoguzov, D. Lucchetti, N. C. Brown, T. M. Gatterman, S. K. Halit, K. Gilmore, J. A. Gerber, B. Neyenhuis, D. Hayes, and R. P. Stutz. Realization of real-time fault-tolerant quantum error correction. *Phys. Rev. X*, 11:041058, Dec 2021.
- [61] J. Hilder, D. Pijn, O. Onishchenko, A. Stahl, M. Orth, B. Lekitsch, A. Rodriguez-Blanco, M. Müller, F. Schmidt-Kaler, and U. G. Poschinger. Fault-tolerant parity readout on a shuttling-based trapped-ion quantum computer. *Phys. Rev. X*, 12:011032, Feb 2022.
- [62] Sergey Bravyi, Andrew W. Cross, Jay M. Gambetta, Dmitri Maslov, Patrick Rall, and Theodore J. Yoder. High-threshold and low-overhead fault-tolerant quantum memory. *Nature*, 627(8005):778–782, 2024.
- [63] Lawrence Z. Cohen, Isaac H. Kim, Stephen D. Bartlett, and Benjamin J. Brown. Low-overhead fault-tolerant quantum computing using long-range connectivity. *Science Advances*, 8(20):eabn1717, 2022.
- [64] Nikolas P. Breuckmann and Jens Niklas Eberhardt. Quantum low-density parity-check codes. *PRX Quantum*, 2:040101, Oct 2021.
- [65] Jeongwan Haah and Matthew B. Hastings. Codes and Protocols for Distilling T, controlled-S, and Toffoli Gates. *Quantum*, 2:71, June 2018.
- [66] Austin G. Fowler, Simon J. Devitt, and Cody Jones. Surface code implementation of block code state distillation. *Scientific Reports*, 3(1):1939, 2013.
- [67] Earl T. Campbell and Mark Howard. Magic state parity-checker with pre-distilled components. *Quantum*, 2:56, March 2018.
- [68] Craig Gidney, Noah Shutt, and Cody Jones. Magic state cultivation: growing t states as cheap as cnot gates, 2024.
- [69] Yu Tomita and Krysta M. Svore. Low-distance surface codes under realistic quantum noise. *Phys. Rev. A*, 90:062320, Dec 2014.
- [70] Poulami Das, Aditya Locharla, and Cody Jones. Lilliput: a lightweight low-latency lookup-table decoder for near-term quantum error correction. In *Proceedings of the 27th ACM International Conference on Architectural Support for Programming Languages and Operating Systems, ASPLOS ’22*, page 541–553, New York, NY, USA, 2022. Association for Computing Machinery.
- [71] Samuel C. Smith, Benjamin J. Brown, and Stephen D. Bartlett. Local predecoder to reduce the bandwidth and latency of quantum error correction. *Phys. Rev. Appl.*, 19:034050, Mar 2023.
- [72] Christopher Chamberland, Luis Goncalves, Prasahnt Sivarajah, Eric Peterson, and Sebastian Grimberg. Techniques for combining fast local decoders with global decoders under circuit-level noise. *Quantum Science and Technology*, 8(4):045011, jul 2023.
- [73] Philip Andreasson, Joel Johansson, Simon Liljestrand, and Mats Granath. Quantum error correction for the toric code using deep reinforcement learning. *Quantum*, 3:183, September 2019.
- [74] P Baireuther, M D Caio, B Criger, C W J Beenakker, and T E O’Brien. Neural network decoder for topological color codes with circuit level noise. *New Journal of Physics*, 21(1):013003, jan 2019.
- [75] Oscar Higgott and Craig Gidney. Sparse blossom: correcting a million errors per core second with minimum-weight matching, 2023.
- [76] Yue Wu and Lin Zhong. Fusion blossom: Fast mwpm decoders for qec, 2023.
- [77] Suhas Vittal, Poulami Das, and Moinuddin Qureshi. Astrea: Accurate quantum error-decoding via practical minimum-weight perfect-matching. In *Proceedings of the 50th Annual International Symposium on Computer Architecture, ISCA ’23*, New York, NY, USA, 2023. Association for Computing Machinery.
- [78] Narges Alavisamani, Suhas Vittal, Ramin Ayanzadeh, Poulami Das, and Moinuddin Qureshi. Promatch: Extending the reach of real-time quantum error correction with adaptive predecoding, 2024.
- [79] Antonio deMarti iOlus, Patricio Fuentes, Román Orús, Pedro M. Crespo, and Josu Etxezarreta Martinez. Decoding algorithms for surface codes. *Quantum*, 8:1498, October 2024.